SPACE-TIME RESIDUAL DISTRIBUTION SCHEMES FOR TWO-DIMENSIONAL EULER AND TWO-PHASE FLOW SIMULATIONS

Árpád Csík, Mario Ricchiuto and Herman Deconinck
VON KARMAN INSTITUTE FOR FLUID DYNAMICS,
Chaussèe de Waterloo, 72
B-1640 Rhode Saint Genèse, Belgium
Email: arpi@vki.ac.be, ricchiut@vki.ac.be, deconinck@vki.ac.be
web page: http://www.vki.ac.be

Abstract. Multidimensional upwind residual distribution schemes are extended to the time accurate solution of systems of hyperbolic conservation laws, based on a consistent discretization of the space-time domain. Due to the upwind property of the schemes and to an appropriate choice of the space-time mesh geometry, the solution is decoupled into temporal slabs, allowing to construct an efficient unconditionally stable implicit time marching procedure, while maintaining full consistency, monotonicity and second order accuracy both in space and time. The method is tested on two-dimensional problems involving the solution of the compressible Euler and Homogeneous Two-Phase flow equations. Numerical results demonstrate the robustness and the accuracy of the method.

Key words: residual distribution method, space-time method, time accurate computations, unsteady Euler, unsteady two-phase flow

1 INTRODUCTION

Over the last decade, a class of upwind spatial discretization techniques, known as fluctuation splitting or residual distribution ($\mathcal{RD}$) schemes has been developed for the numerical solution of systems of hyperbolic conservation laws on unstructured grids [1,2,3]. The method operates on triangles and tetrahedra, in two and three spatial dimensions, respectively. It incorpo-

rates the same upwind properties at the basis of Godunov type finite volume schemes, but carried over to a cell vertex framework with a continuous piecewise linear representation of the solution, like in finite element methods.

The main advantage of the $\mathcal{RD}$ approach is that both a monotonic resolution of discontinuities, and second order of accuracy in smooth *steady* flows can be achieved for arbitrary unstructured grids, on the compact stencil of the nearest neighbors. The latter property enables an efficient implicit and parallel implementation. Another attractive feature of the method is that true multidimensional information derived from the physics of the problem is incorporated into the upwinding procedure.

However, these schemes have been developed for the solution of steady state problems and the second order accuracy degrades to first order, when they are used in combination with the method of lines (such as Runge-Kutta schemes) for the computation of unsteady flows. Second order spatial accuracy can be recovered if a consistent mass matrix formulation is applied for the temporal derivative (hence leading to an implicit scheme), similar to what is required in stabilized finite element methods. Another route to second order of accuracy in space and time is the Taylor-Galerkin approach, equivalent to the Lax-Wendroff scheme in its simplest setting. Unfortunately, in both cases the resulting discretization is non-positive and oscillatory solutions are obtained in the presence of discontinuities. Some cures to this problem have been investigated, *e.g.* applying a Flux Corrected Transport (FCT) technique [4]. In this approach a monotone first order and a non-monotone second order schemes are combined to obtain a high order non-linear monotone scheme [1,5,6,7]. However, experience has shown that a Flux Corrected Transport approach as a cure to recover monotonicity for systems lacks robustness. Moreover, using FCT as a way to stabilize a characteristic based upwind scheme is very unsatisfactory from the theoretical point, especially in combination with the mass-matrix approach.

A more attractive framework might be to consider space-time methods, as *e.g.* applied in the context of stabilized finite element methods [8] or discontinuous Galerkin methods [9,10,11]. More recently, Abgrall [1,12] proposed a *continuous* space-time formulation of the $\mathcal{RD}$ method in two spatial dimensions. The solution representation is based on a bilinear interpolation over prismatic elements which are triangular in space and linear in time. The approach allows to decouple the space-time domain into temporal slabs of one

single row of elements per time step, thus effectively resulting in a implicit time-marching procedure. Unfortunately, the positivity of Abgrall's implicit schemes requires the satisfaction of an explicit type time step limitation.

In the present paper we elaborate on the idea of a linear *continuous* space-time residual distribution. We use the standard schemes operating on piecewise linear elements, developed in the past, applying them to the solution of *unsteady* problems on space-time meshes [14,15]. The intrinsic upwinding property of these schemes is used to decouple the solution on the entire space-time domain in a sequence of temporal slabs containing two layers elements. It turns out that the decoupling (past shielding) can only be obtained if the mesh satisfies certain geometric properties, *and* if the time step for the first layer is limited by a CFL type condition as in Abgrall's approach. However, since no past shielding is needed for the second layer, arbitrary CFL numbers can be obtained, while maintaining second order of accuracy and monotonicity both in space and time.

The paper is organized as follows: in section 2 we describe the space-time formulation of standard residual distribution schemes. The particular geometry of the space-time grid and the past shielding condition are discussed in section 3. Results of several Euler computations are presented in section 4, while in section 5 we deal with the solution of the Homogeneous Two-Phase flow equations. In the last section conclusive remarks and future perspectives are given.

2 DISCRETIZATION IN SPACE-TIME

We consider a system of hyperbolic conservation laws consisting of q equations in d spatial dimensions over space-time domain Ω:

$$\frac{\partial U}{\partial t} + \nabla \cdot \mathbf{G} = 0, \qquad \text{for } \forall (\mathbf{x}, t) \in \Omega, \tag{1}$$

where U is the vector of conserved variables and $\mathbf{G}$ is the $q \times d$ flux function. The quasilinear form of equation (1) is:

$$\frac{\partial U}{\partial t} + \left(\frac{\partial G_m}{\partial U} \hat{\mathbf{x}}_m \right) \cdot \nabla U = 0. \tag{2}$$

In equation (2) and in the rest of this paper, index $m = [1, ..., d]$ refers to the Einstein summation convention and $\hat{\mathbf{x}}_m$ is the unit vector in the m-th

spatial direction. The unit vector in time is denoted by $\hat{\mathbf{t}}$. Using space-time notation, system (1) can be rewritten as:

$$\vec{\nabla} \cdot \vec{\mathbf{F}} = 0, \tag{3}$$

where the space-time flux vector $\vec{\mathbf{F}}$ and the nabla operator $\vec{\nabla}$ are:

$$\vec{\mathbf{F}} = \mathbf{G} + U\,\hat{\mathbf{t}} \quad \text{and} \quad \vec{\nabla} = \nabla + \hat{\mathbf{t}}\frac{\partial}{\partial t}. \tag{4}$$

In the following, we limit ourselves to the case of two spatial dimensions. The corresponding three-dimensional space-time domain is divided into non-overlapping tetrahedra. The solution U is approximated in the continuous, piecewise linear finite element space:

$$U(\mathbf{x}, t) = \sum_{j=1}^{N} U_j w_j(\mathbf{x}, t), \tag{5}$$

where U_j is the discrete solution at node j, $w_j(\mathbf{x}, t)$ is the piecewise linear finite element shape function and N is the total number of nodes in the space-time mesh.

In element E the cell residual Φ^E is defined as:

$$\Phi^E = \oint_{\partial E} \vec{\mathbf{F}} \cdot \vec{\mathbf{n}}\, dS = \left(\frac{\partial \bar{G}_m}{\partial U}\, \hat{\mathbf{x}}_m + \hat{I}\,\hat{\mathbf{t}} \right) \cdot \int_E \vec{\nabla} U\, d\Omega, \tag{6}$$

where $\vec{\mathbf{n}}$ is the outward pointing unit normal of surface element dS and $\partial \bar{G}_m / \partial U$ is the m-th component of the flux Jacobian evaluated in an averaged state $\bar{U}$ chosen such that equation (6) holds exactly at the discrete level [13].

Let $\vec{\mathbf{n}}_i = n_m^i \hat{\mathbf{x}}_m + n_t^i\,\hat{\mathbf{t}}$ be the inward pointing vector normal to the face opposite to node i in element E (see figure 1). Introducing the following linear combination of the space-time Jacobian matrices:

$$K_i = \frac{1}{d+1} \left(\frac{\partial \bar{G}_m}{\partial U}\, n_m^i + \hat{I}\, n_t^i \right), \tag{7}$$

the cell residual can be written in the following compact form:

$$\Phi^E = \sum_{i=1}^{d+2} K_i U_i. \tag{8}$$

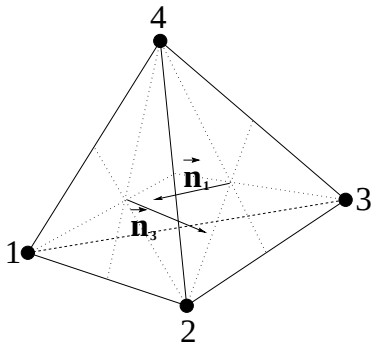

Figure 1: Tetrahedral element with inward pointing scaled normals

Since system (1) is hyperbolic, the q eigenvalues of matrix K_i are real, and a complete set of q real linearly independent eigenvectors exists. The diagonalization of matrix K_i yields: $K_i = R_i \Lambda_i L_i$, where Λ_i is the eigenvalue matrix, the columns of R_i contain the right eigenvectors and $L_i = (R_i)^{-1}$. The eigenvalue matrix can be decomposed as $\Lambda_i = \Lambda_i^+ + \Lambda_i^-$, where

$$\Lambda_i^{\pm} = \frac{\Lambda_i \pm |\Lambda_i|}{2}. \tag{9}$$

The generalized upwind parameters K_i^+ and K_i^- defined as

$$K_i^+ = R_i \Lambda_i^+ L_i \quad \text{and} \quad K_i^- = R_i \Lambda_i^- L_i, \tag{10}$$

play an important role in the multidimensional upwind property of the system residual distribution schemes. In element E, node i does not receive any contribution from the cell residual if all the eigenvalues of the corresponding matrix K_i are non-positive, *i.e.* Λ_i^+ is the null matrix. The distribution function Φ_i^E is the fraction of the cell residual Φ^E distributed to node i in element E. For consistency we require that

$$\sum_{i=1}^{d+2} \Phi_i^E = \Phi^E. \tag{11}$$

We consider three different schemes, the first order positive linear N scheme, the second order linear LDA scheme and the second order positive nonlinear

B scheme. The corresponding distribution functions are defined by:

$$\begin{aligned}
&\Phi_i^N = K_i^+(U_i - U_{in}), && U_{in} = \left(\sum_{i=1}^{d+2} K_i^-\right)^{-1} \sum_{i=1}^{d+2} K_i^- U_i, \\
&\Phi_i^{LDA} = \beta_i^{LDA}\Phi^E, && \beta_i^{LDA} = K_i^+ \left(\sum_{i=1}^{d+2} K_i^+\right)^{-1}, \\
&\Phi_i^B = \Theta\Phi_i^N + (1-\Theta)\Phi_i^{LDA}, && \Theta_{j,j} = \frac{|\Phi_j^E|}{\sum_{k=1}^{d+2} |\Phi_{k,j}^N|}.
\end{aligned} \tag{12}$$

Assembling the contributions Φ_i^E from all the elements E to the nodes, the nodal values of the unknown U_i in the space-time mesh are the solution of the algebraic system of equations:

$$\sum_{E, i\in E} \Phi_i^E = 0 \quad \forall i \in [1, ..., N]. \tag{13}$$

In the present work we use explicit iterations in pseudo time to solve the implicit system for each physical time step. Typically $10-50$ explicit iterations are needed to converge the solution in pseudo time.

3 SPACE-TIME GEOMETRY

In order to design an efficient time marching procedure, the full space-time solution of the problem has to be decoupled into temporal slabs. Upwind $\mathcal{RD}$ schemes operating on properly designed space-time grids naturally lead to this decoupling. We propose a space-time mesh geometry containing three levels of nodes and two layers of elements in the temporal direction. The first, second, and third levels of nodes have temporal coordinates t_n, $t_{n+1/2}$, and t_{n+1}, and will be called respectively *past*, *intermediate* and *future* time levels. The time steps corresponding to the first and second layers are denoted by $\Delta t_1 = t_{n+1/2} - t_n$ and $\Delta t_2 = t_{n+1} - t_{n+1/2}$, respectively. The space-time solution is decoupled if no residual contribution is sent to the nodes located at the *past* level, *i.e.* past nodes are shielded against artificial propagation of information backward in time. In this paper the past shield condition is described for a 2D scalar conservation law. More details on the extension to hyperbolic systems can be found in [14,15].

Consider the following 2D scalar hyperbolic problem:

$$\frac{\partial u}{\partial t} + \bar{\lambda} \cdot \nabla u = 0, \text{ for } \forall (\mathbf{x}, t) \in \Omega, \tag{14}$$

where $\bar{\lambda}$ is the locally linearized advection speed vector. For a given triangulation of the 2D spatial domain a particular space-time grid is generated containing two layers of tetrahedra. The first layer consists of three types of elements (see figure 2). Type E1 has three past nodes situated at level n, and one node at the intermediate level $n + 1/2$. The spatial position of the intermediate node is at the mass center of the base triangle in the past plane. Type E2 has two past and two intermediate nodes. Finally, type E3 has one past node and three intermediate nodes. The second layer is obtained by mirroring the first one with respect to the intermediate plane and stretching it in the temporal direction according to the ratio $Q = \Delta t_2/\Delta t_1$.

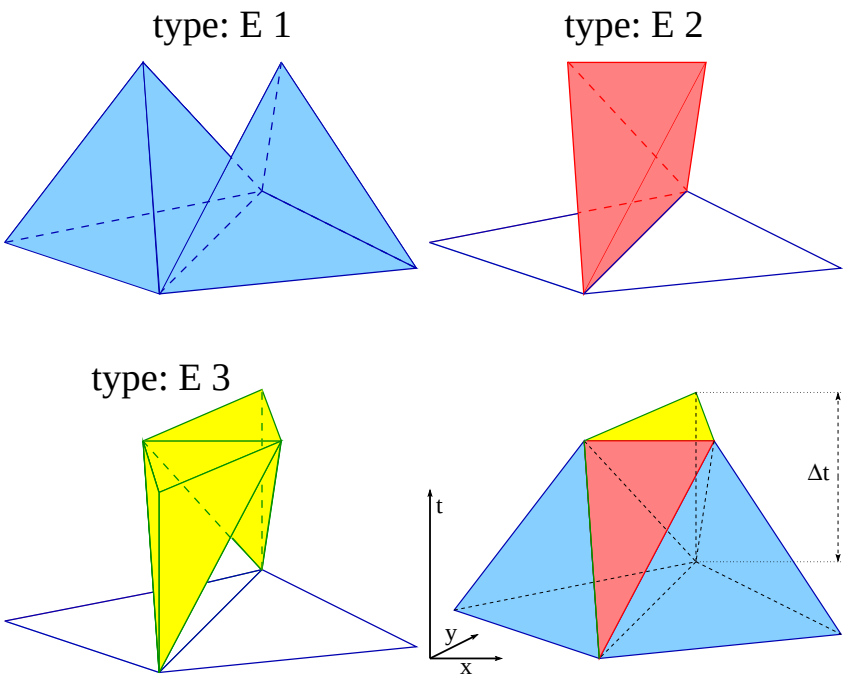

Figure 2: Three types of basic tetrahedra used to build the first layer of the space-time mesh in two spatial dimensions, and the schematic view of the mesh.

The past shield condition translates into the constraint that no residual has to be sent to the past nodes of elements E1, E2 and E3. It is straightforward to verify that in elements of type E3 no residual is sent to the unique past node by any of the schemes introduced in the previous section. Considering elements of type E1, let us define the triangle T_j^S as the projection of the face opposite to node j onto the past plane. Using the notation of figure 1 the past shield condition for all the three past nodes leads to the following constraint on the time step Δt_1^{E1} associated to the element:

$$CFL_1^{E1} = \max_{j=1,2,3} \left(\frac{k_j^+ \, \Delta t_1^{E1}}{S_{T_j^S}} \right) < 1, \tag{15}$$

where $S_{T_j^S}$ is the area of T_j^S, $k_j^+ = \max(0, k_j)$ and

$$k_j = \frac{\bar{\lambda} \cdot \tilde{\mathbf{n}}_j}{2},$$

which is the scalar upwind parameter corresponding to vertex j of the base triangle (i.e. $\tilde{\mathbf{n}}_j$ is scaled with the length of the edge opposite to j in the base triangle of the initial spatial triangulation). A similar constraint is obtained for the time step Δt_1^{E2} associated to elements of type E2. The time step Δt_1 is obtained as

$$\Delta t_1 = \min \left(\Delta t_1^{E1}, \Delta t_1^{E2} \right).$$

Since Δt_2 is not restricted by any conditions, arbitrarily large global time steps can be obtained according to

$$\Delta t = \Delta t_1 + \Delta t_2 = (Q+1) \Delta t_1. \tag{16}$$

For the extension of the analysis to the system case see references [14,15].

4 NUMERICAL RESULTS: EULER EQUATIONS

The Euler equations describe the dynamics of compressible inviscid fluids. In their conservative form (1) the state vector U and the flux function $\mathbf{G}$ are given by:

$$U = \begin{pmatrix} \rho \\ \rho \mathbf{v} \\ E \end{pmatrix} \quad \text{and} \quad \mathbf{G} = \begin{pmatrix} \rho \mathbf{v} \\ \rho \mathbf{v}\mathbf{v} + \hat{I} p \\ (E+p)\mathbf{v} \end{pmatrix}, \tag{17}$$

where ρ is the density, $\mathbf{v}$ is the velocity vector, p is the thermal pressure and E is the total energy density. We present the results of three test-cases in two spatial dimensions, *i.e.* the interaction of linear sound waves, a 2D Riemann Problem and the Mach 3 flow in a channel with a forward facing step proposed by Colella an Woodward [16].

Interaction of Linear Sound Waves

This test case concerns the propagation and interaction of linear sound waves over a static background. In the initial state two exponentially decaying axisymmetric pressure perturbations with a maximum amplitude of $\delta p = 0.1$ are superposed onto a static background with $\rho = 140$, $\mathbf{v} = 0$, and $p = 100$. In the solution of this problem the pressure perturbations are carried away by linear waves propagating with the speed of the sound. In figure 3 we show a series of snapshots at different time steps computed by the second order linear LDA scheme on a mesh containing 101×101 points in space. On the last two plots the interference of the two waves can be observed. This test case illustrates the robustness of the space-time method for problems involving static regions without the need of any special treatment.

A 2D Riemann Problem

To further validate the method in two spatial dimensions we propose a 2D Riemann problem. At $t = 0$ a squared shaped $[3.6 \times 3.6]$ uniform domain with $\rho_1 = 3$, $\mathbf{v_1} = 0$ and $p_1 = 3$ is embedded into an infinite uniform domain with $\rho_2 = 1$, $\mathbf{v}_2 = 0$ and $p_2 = 1$. For symmetry reasons it is sufficient to compute the solution over one quarter of the full domain. The solution is computed at $t = 0.4$ on a structured triangulation of the 2D spatial domain containing 101×101 points in space ($\Delta x = \Delta y = 0.02$). The density and pressure surfaces are shown in figure 4. for the first order N and the second order B schemes. The shock, shear and the expansion are well resolved in both spatial directions. Since at $t = 0.4$ the corner effect of the 2D Riemann problem has not reached the boundaries of the computational domain, the solution along the coordinate axes is identical to the solution of the 1D Riemann problem with the same initial data. In figure 5 we show a comparison between the density computed by the 1D space-time schemes (on a mesh with the same spacing) and the cut along the x-axis of the 2D computations for both for the N and B schemes. We observe that the numerical solutions match with a high accuracy in the case of the second order B scheme. The first order N scheme is more dissipative in 2D.

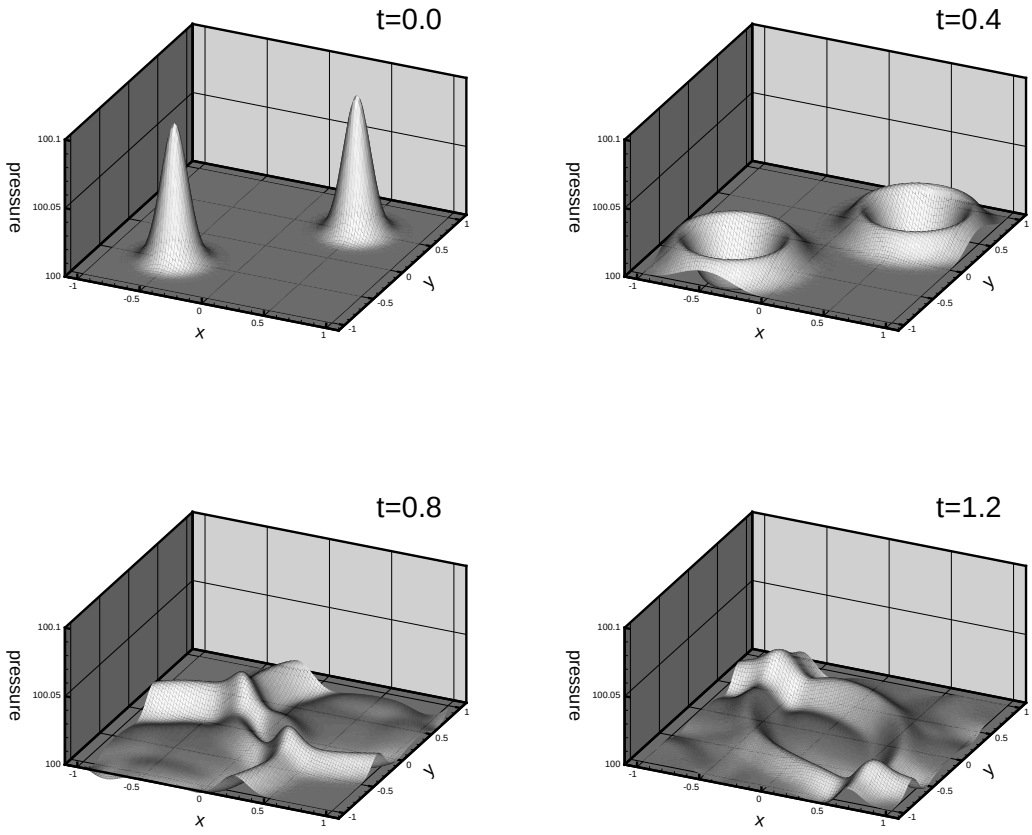

Figure 3: Interaction of linear sound waves. Four snapshots of the pressure surface for a mesh containing 101×101 nodes. Computation made by the second order linear LDA scheme.

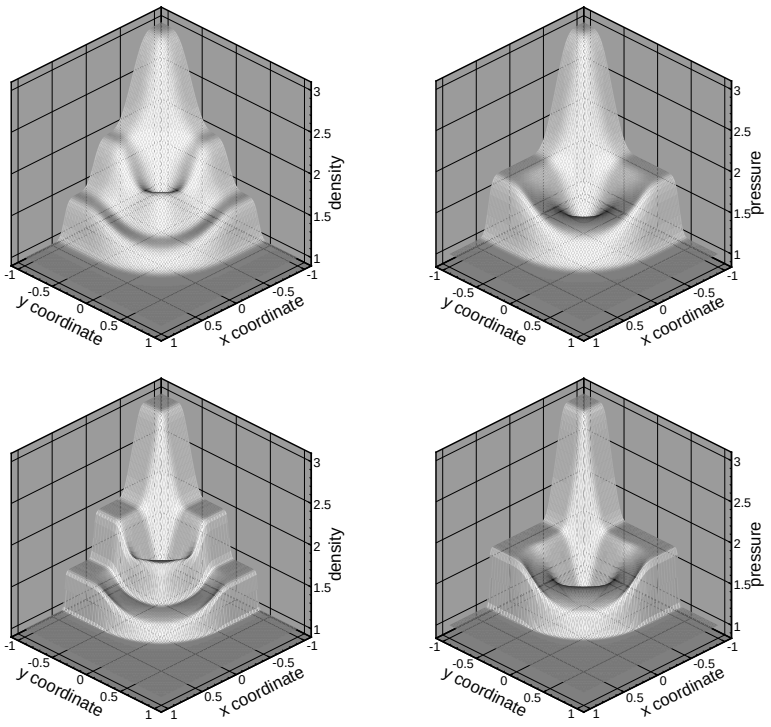

Figure 4: 2D Riemann problem: $t = 0.4$. Top: N scheme. Bottom: B scheme.

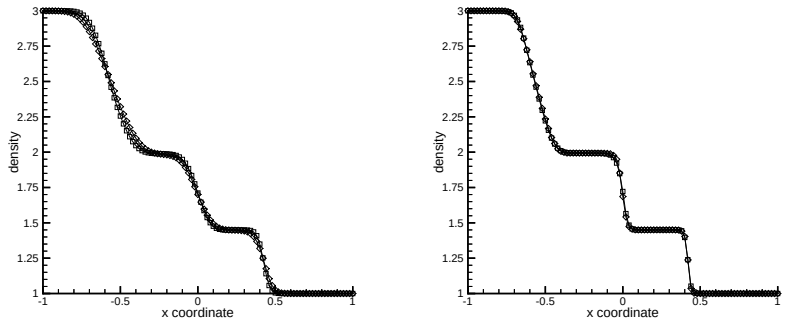

Figure 5: 2D Riemann problem: profile of the density at $t = 0.4$. Squares: true 1D solution. Diamonds: 2D solution along the x-axis. Left: N scheme. Right: B scheme.

Mach 3 Wind Tunnel with a Forward Facing Step

To illustrate the benefit of the unconditionally stable implicit $\mathcal{RD}$ schemes, we compute the test case proposed by Colella and Woodward [16]. The spatial mesh is a uniform triangulation of the domain with average size of the triangles given by $h = 1/80$, except for the corner of the step, where a severe local refinement was used, as shown in figure 6. This refinement is necessary to limit the numerical entropy production at the corner, see also [10] for more details. In total the spatial mesh contains 38,740 triangles and 19,715 nodes.

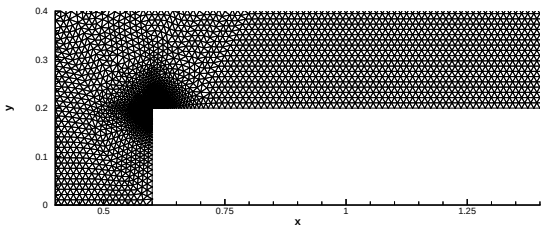

Figure 6: Mach 3 flow over a forward facing step. Part of the unstructured grid close to the corner of the step.

The computation is performed by the second order nonlinear B scheme. The global time step is chosen such that $CFL \approx 1$ for the triangles in the uniform region. However, in the corner region this amounts to a local value of $CFL \approx 12$, due to the small size of the cells in this area. This clearly shows the benefit of an unconditionally stable implicit scheme, even for unsteady computations. Isolines of the density at different instances in time are presented in figure 7, and compared with the solution of Colella and Woodward [16]. This reference solution was computed by a third order PPM method on a uniform mesh containing quadrilaterals of size $h = 1/80$ (note that in the reference computation the entropy was fixed at the corner in order to avoid the artificial entropy generation).

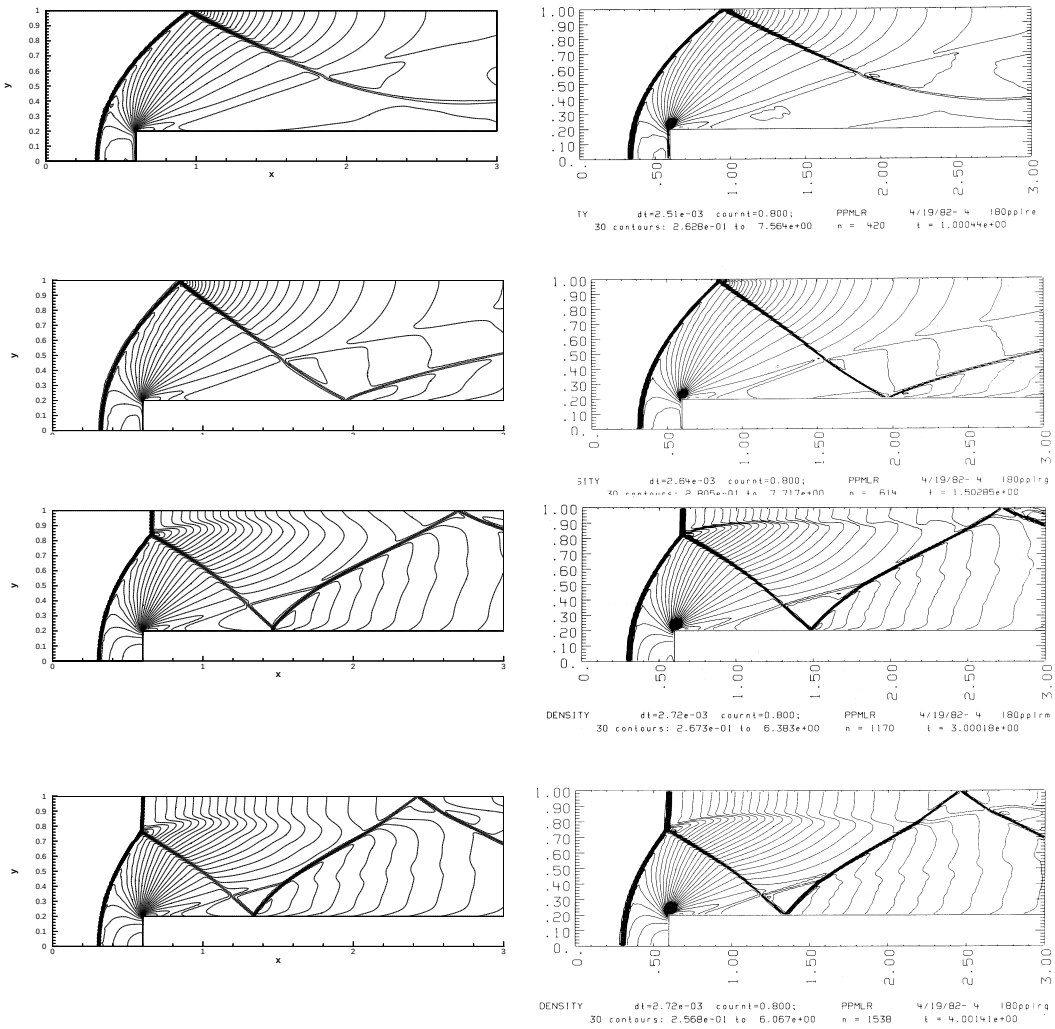

Figure 7: Density isolines of a Mach 3 flow in a wind tunnel with a forward facing step. Left: second order space-time B scheme. Right: third order reference solution [16]. From top to bottom: $t = 1.0, t = 1.5, t = 3.0, t = 4.0$.

5 NUMERICAL RESULTS: TWO-PHASE FLOW EQUATIONS

In this section the space-time method is applied to the simulation of unsteady gas liquid two-phase flows. In particular, we employ the homogeneous isentropic model given by the following hyperbolic system:

$$\frac{\partial U}{\partial t} + \nabla \cdot \mathbf{G} = Q, \qquad \text{for } \forall (\mathbf{x}, t) \in \Omega, \tag{18}$$

where the state vector U and the flux function $\mathbf{G}$ are given by:

$$U = \begin{pmatrix} \alpha_l \rho_l \\ \alpha_g \rho_g \\ \rho \mathbf{v} \end{pmatrix}, \qquad \mathbf{G} = \begin{pmatrix} \alpha_l \rho_l \mathbf{v} \\ \alpha_g \rho_g \mathbf{v} \\ \rho \mathbf{v}\mathbf{v} + \hat{I} p \end{pmatrix}, \tag{19}$$

and the source term Q describes the effect of gravity:

$$Q = \begin{pmatrix} 0 \\ 0 \\ \rho \mathbf{g} \end{pmatrix}. \tag{20}$$

In equations (19) and (20) α_g is the gas or *void* fraction (volume concentration), α_l is the liquid fraction, $\mathbf{v}$ is the velocity vector, ρ is the mixture density and $\mathbf{g}$ is the gravitational acceleration. The model is closed by the following equations:

$$\begin{aligned} \rho &= \alpha_l \rho_l + \alpha_g \rho_g, \\ \alpha_l &= 1 - \alpha_g, \\ \rho_l &= \rho_{l0} + \tfrac{p - p_0}{a_l^2}, \\ p &= \Gamma_g \rho_g^{\gamma_g}. \end{aligned} \tag{21}$$

System (18) has been solved by the space-time B scheme and an upwind treatment of the source term Q. Details regarding the source term discretization will be given in a forthcoming paper. More information related to the two-phase flow modeling are given in references [17,18,19].

Sloshing of a Water Column in a Tank

This is a very common benchmark test for two-phase flow codes. The problem consists of a liquid column initially at rest in hydrostatic equilibrium in a tank. The initial height and width of the water column are $2L$ and L respectively. The length of all the sides of the tank is $4L$ and its top side is open to the atmosphere.

At time $t = 0$ the water column is released and starts to move due to the effect of gravity. The water flows toward to opposite end of the tank until it splashes against the wall and then it moves back. The problem has been studied both numerically and experimentally [17,20,21]. In particular, experimental data are available in literature for the position of the leading edge of the moving liquid front. The distance of the front from the left wall of the tank Z scaled by the initial width of the water column L is given as a function of the reduced time t^* defined as:

$$t^* = t\sqrt{2g/L}\ . \tag{22}$$

The width of the initial water column is $L = 0.146$ m. The same value was used in the experiments of Koshizuka *et al.* [21]. Unfortunately, due to the numerical diffusion the interface between the phases is spread over several computational cells. Consequently, the precise position of the interface is hard to define. To compare with the experimental data in [20,21] we assume that the interface is located at the position where the gas void fraction is $\alpha_g = 0.5$.

In the computations the mesh is an isotropic Delaunay triangulation containing 11804 nodes and 23206 triangles. The CFL number was fixed to 100. The unsteady motion of the liquid starting from its initial position is visualized in figures 8, 9 and 10 by plotting the shaded isolines of the gas void fraction at different instants. The pure liquid and the gas phases are indicated by blue and red colors respectively.

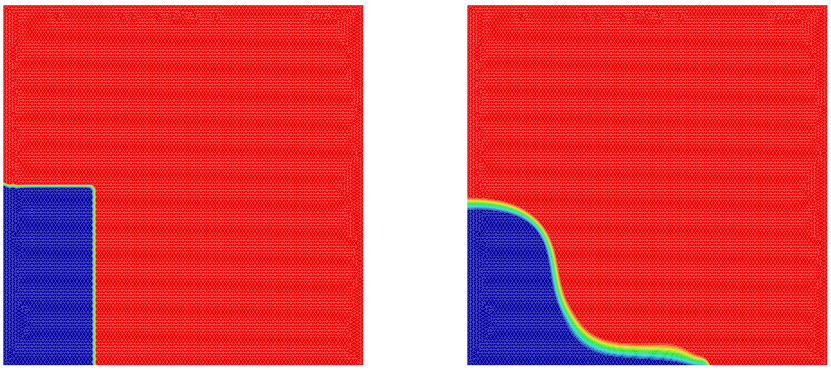

Figure 8: Sloshing of a water column in a tank. Void fraction contours computed by the B Scheme. Left: $t^* = 0$. Right: $t^* \approx 2.5$.

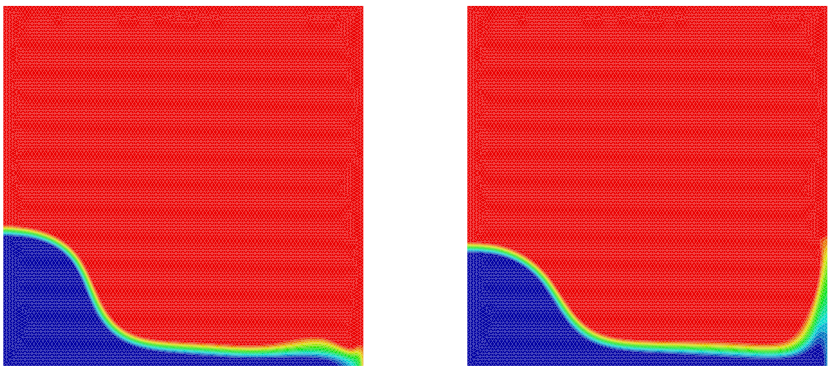

Figure 9: Sloshing of a water column in a tank. Void fraction contours computed by the B Scheme. Left: $t^* \approx 3.7$. Right: $t^* \approx 4.4$.

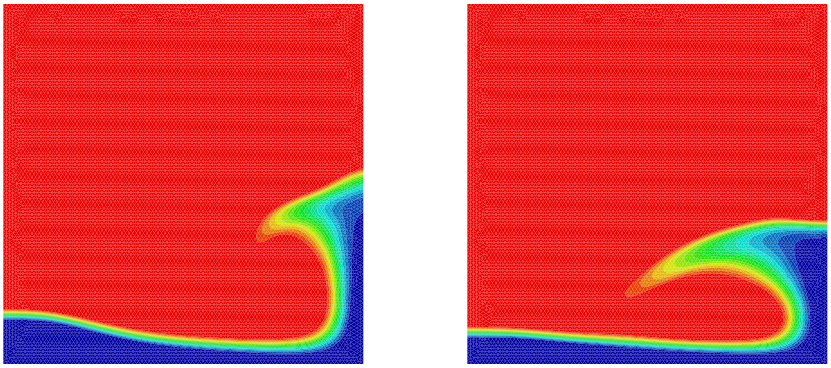

Figure 10: Sloshing of a water column in a tank. Void fraction contours computed by the B Scheme. Left: $t^* \approx 7.5$. Right: $t^* \approx 9$.

On the left in figure 11 we present the streamline pattern at $t^* \approx 9$ superimposed onto the shaded contour plot of the gas void fraction. Three main recirculating regions are visible in correspondence to the gas-liquid interface. This is a direct consequence of the main assumption at the basis of model (18), that the two phases have the same velocity everywhere corresponding to an infinite viscous drag acting at their interface. Finally, on the right of the same figure we show the comparison of the computed liquid front position with the experimental data of [20,21]. The numerical results properly predict the parabolic behavior obtained by the experiments. At the earlier times the

agreement is particularly good. However, after $t^* \approx 2$ the numerical values deviate from the experimental ones. The reason could be the poor modeling of the physics. Indeed, the model considered is one of the simplest, since it does not include viscous effects and both the action of the surface tension and eventual mechanical non-equilibrium due to non-zero relative velocity are neglected.

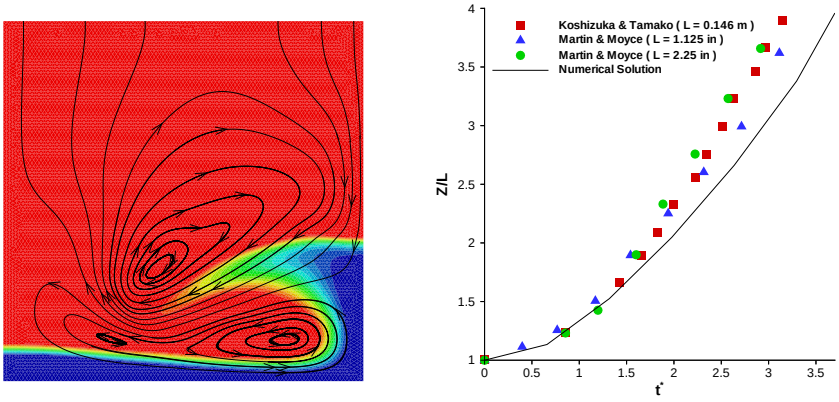

Figure 11: Sloshing of a water column in a tank. Left: void fraction and streamlines at $t^* \approx 9$. Right: comparison with experimental data.

6 CONCLUSIONS

Multidimensional upwind residual distribution schemes have been extended to the context of linear space-time elements for the approximation of the unsteady solution of hyperbolic systems of conservation laws. Positivity and linearity preservation of the original schemes are carried over to the full space-time solution, *i.e.* the linearity preserving schemes retain second order accuracy in smooth flows and the positive schemes resolve discontinuities without spurious oscillations both in space and time.

Due to the intrinsic upwinding properties of the standard $\mathcal{RD}$ schemes, the space-time solution is decoupled onto a sequence of temporal slabs containing two layers of elements. Although, in the first layer an explicit type CFL condition has to be respected, in the second layer arbitrary time steps can be taken.

The robustness and reliability of the approach has been demonstrated on a wide range of applications. Compared to most common implicit time-integrators the main disadvantage of the space-time method concerns the increases computational cost and the higher memory requirements. Nevertheless, its great potential for the solution of time dependent problems, especially involving moving boundaries, is indisputable.

8 REFERENCES

[1] H. Deconinck, K. Sermeus and R. Abgrall "Status of Multidimensional Upwind Residual Distribution Schemes and Application in Aeronautics", *AIAA-CP 2000-2328* (2000)

[2] H. Paillère, H. Deconinck and P.L. Roe "Conservative Upwind Residual Distribution Schemes Based on the Steady Characteristics of the Euler Equations", *AIAA-CP 95-1700* (1995)

[3] E. var der Weide, H. Deconinck, E. Issmann and G. Degrez "Fluctuation Splitting Schemes for Multidimensional Convection Problems: an Alternative to Finite Volume and Finite Element Methods", *Computational Mechanincs*, Vol. 23, No. 2, 199–208 (1999).

[4] R. Lohner, K. Morgan, J. Peraire and M. Vahdati "Finite Element Flux-Corrected Transport for the Euler and Navier-Stokes Equations", *International Journal for Numerical Methods in Fluids*, Vol. 7, 1093–1109 (1997).

[5] A. Ferrante and H. Deconinck "Solution of the Unsteady Euler Equations using Residual Distribution and Flux-Corrected Transport", *PR1997-08*, von Karman Institute (1997)

[6] M.E. Hubbard and P.L. Roe "Compact High-Resolution Algorithms for Time-Dependent Advection on Unstructured Grids", *International Journal for Numerical Methods in Fluids*, Vol. 33, No. 5, 711–736 (2000)

[7] M. Ricchiuto and H. Deconinck "Time Accurate Solution of Hyperbolic Partial Differential Equations using FCT and Residual Distribution", *SR1999-33*, von Karman Institute (1999)

[8] C. Johnson "The Streamline Diffusion Finite Element Method for Compressible and Incompressible Flow", *Lecture Series: Computational Fluid Dynamics*, von Karman Institute (1990).

[9] R.B. Lowrie, P.L. Roe and D. van Leer "Space-Time Methods for Hyperbolic Conservation Laws", *Barrier and Challenges in Computational Fluid Dynamics*, Kluwer Academic Publishers (1998)

[10] B. Cockburn, "Discontinuous Galerkin Methods for Convection Dominated Problems", *High-Order Methods for Computational Physics*, editors T.J. Barth and H. Deconinck, Springer (1999)

[11] P. Hansbo, "The Characteristic Streamline Diffusion Method for Convection-Diffusion Problems", *Computer Methods in Applied Mech. and Eng.*, Vol. 96, 239–253 (1992)

[12] R. Abgrall and M. Mezine "A Consistent Upwind Residual Scheme for Unsteady Advection Problems", *AMIF Conference*, Italy (2000)

[13] H. Deconinck, P.L. Roe and R. Struijs "A Multidimensional Generalization of Roe's Flux Difference Splitter for the Euler Equations", *Computers and Fluids*, Vol. 22, 215–222 (1993)

[14] Á, Csík, M. Ricchiuto, H. Deconinck and S. Poedts "Space-Time Residual Distribution Schemes for Hyperbolic Conservation Laws", *AIAA-CP 2001-2617* (2001)

[15] Á, Csík and H. Deconinck "Space-Time Residual Distribution Schemes for Hyperbolic Conservation Laws on Unstructured Linear Finite Elements", *ICFD Conf. Proc.* (2001), accepted for publication in the *International Journal for Numerical Methods in Fluids*

[16] P. Colella and P. Woodward "The Numerical Simulation of Two-Dimensional Fluid Flow with Strong Shocks", *Journal of Computational Physics*, Vol. 54, 115–173 (1984)

[17] E. Valero "Advanced 2D Two-Phase Flow Simulation Tool for Application to Reactor Safety", *VKITN2001-198*, von Karman Institute (2001)

[18] M. Ricchiuto, Á, Csík and H. Deconinck "Space-Time Residual Distribution Schemes and Application to Unsteady Two-Phase Flow Computations on Unstructured Meshes", *VKIPR2001-23*, von Karman Institute (2001)

[19] I. Toumi, A. Kumbaro and H. Paillére "Approximate Riemann Solvers and Flux Vector Splitting Schemes for Two-Phase Flow", *30^{th} Lecture Series in Computation Fluid Dynamics*, von Karman Institute (1999)

[20] J.C. Martin and W.J. Moyce "An Experimental Study of the Collapse

of Liquid Columns on a Rigid Horizontal Plane", *Phils. Trans R. Soc. Lond*, Vol. 244, 1952

[21] S. Koshizuka, H. Tamako and Y. Oka "A Particle Method for Incompressible Viscous Flow with Fragmentation", *Journal of Computational Fluid Dynamics*, Vol. 4 (1995)